Received: 23 November 2022 | Revised: 16 January 2023 | Accepted: 7 February 2023

IET Energy Systems Integration

DOI: 10.1049/esi2.12095

ORIGINAL RESEARCH

Energy and power management system for microgrids of large-scale building prosumers

Dimitra G. Kyriakou | **Fotios D. Kanellos**

School of Electrical and Computer Engineering, Technical University of Crete, Chania, Greece

Correspondence
Fotios D. Kanellos.
Email: fkanellos@tuc.gr

Abstract

A method for optimal energy and power management of microgrids consisting of mega buildings, plug-in electric vehicles (PEVs) and renewable energy sources (RES) with low computation requirements is proposed by the authors. Thermal and electrical loads are considered for the operation scheduling of the microgrid. In case of non-interconnected operation of the microgrid with the main power grid, the proposed method allows the microgrid to meet the power demand by the buildings and distribution loads exploiting only the hosted PEVs, the integrated RES and, if it is necessary or financially optimal, building auxiliary diesel generators. The primary goal of the suggested algorithm is to significantly reduce the overall daily cost of the microgrid's operation while simultaneously meeting a wide range of constraints. The implementation of the method is based on the exploitation of a two-level hierarchical multi-agent system (MAS) at the level of the microgrid. Suitably defined flexibilities of the microgrid's components to change their power are used to implement optimal power dispatch to them. Detailed simulation results indicated that a remarkable cost reduction of 27% can be achieved.

KEYWORDS

building management systems, electric vehicles, energy consumption, energy management systems, optimisation, particle swarm optimisation, smart power grids

1 | INTRODUCTION

The significant growth in building sector energy consumption and the continuously changing energy sector entails direct intense economic and environmental consequences. In that sense, the optimisation of microgrids' operation scheduling comprising large-scale buildings is becoming an emerging topic of high research interest. In addition to the grid-connected mode of operation, microgrids are capable of operating independently. A remarkable development full of many new prospects and challenges for energy management and control of microgrids is favored by the rapid integration of electric vehicles (EVs). In addition, bi-directional charging stations operating under the Vehicle-to-Grid (V2G) technology will be able to inject electric energy to the microgrid. Consequently, microgrids comprising EVs may present increased resilience during grid outages without necessitating an additional investment in local power generation units.

Energy management systems (EMS) for buildings are mainly limited to the optimisation of single buildings [1–3] instead of microgrids comprising buildings. Research on building EMS has paid more attention to the residential buildings [4–6] than the commercial ones.

Another dimension of the state of the art in building energy system modeling concerns building load modelling. The majority of the works do not take into account either the loads from electric vehicles [7] or the V2G operation [8, 9]. In several cases, focus is specifically placed on the control and modelling of either thermal or electrical loads [10, 11]. In contrast [12, 13], where microgrid islanded operation is not considered, microgrid autonomous or grid-connected mode is optimised in Ref. [14–16]. In Ref. [17–19], optimal energy consumption management by controlling HVAC systems of commercial buildings is examined. Building thermal behavior is modeled and the indoor comfort conditions for the occupants are ensured. In Ref. [20], shiftable heating, cooling and

electrical loads are considered and load shifting is carried out due to its importance for the demand-side response. Moreover, the EMS proposed in Ref. [21] includes the thermal loads of a commercial building and addresses their electrical loads as critical and non-critical. The electric grid has been also modeled in this study and all grid constraints are satisfied. However, the proposed system does not comprise any distributed power generation units or energy storage devices as the building EMS is proposed in Ref. [22, 23].

Significant research has been done so far in coordinated charging control of PEVs, considering their impact on distribution networks. In Ref. [24], the PEVs are simulated as an energy storage system capable of absorbing and supplying active power. However, the main electric grid has not been modeled in this work. The arrival time of the PEVs is a stochastic variable, the departure time is a deterministic one and the different types of building loads have not been modeled separately. In Re. [25], the proposed optimisation model is implemented in an office building microgrid connected to the main grid and considers PEVs and batteries as flexible power demand resources. PEVs have been used as dynamic energy storage system. The optimal scheduling of the power that the EVs should exchange with the electric grid depends on the electricity price and RES generation. Moreover, EVs' travelling patterns, power-SoC dynamics and energy storage systems constraints are used in this work. Despite the extended research in PEV coordinated management and control, there is a research gap in the development of methods exploiting efficient equivalent aggregate battery models for large PEV populations that guarantee rapid convergence and small computation time. These models should be developed in a way that makes them suitable for on-line application. Additionally, there is a need for the development of suitable real-time algorithms for optimal dispatch of the power setpoint of the PEV cluster to its PEVs.

Organisation of building prosumers into microgrids [24, 25] and the applied power and energy management techniques is another important research aspect. Although many research studies have been conducted for the power management of small to medium size buildings [1–6], similar efforts for large-scale commercial buildings, which are more challenging to optimise due to their complexity, are extremely rare. Moreover, online optimisation algorithms based on efficient and simple models that provide optimal scheduling and real-time management and control of large-scale buildings with guaranteed and rapid convergence, satisfying a vast number of constraints, cannot be easily found in the literature.

The innovative features of the proposed method are listed as follows:

- It can be applied to highly complex systems comprising complexes of buildings with hundreds of floors and charging stations hosting thousands of PEVs while low computation time is needed.
- A series of microgrid operations like the operation of building HVAC systems and building non-critical electrical loads, auxiliary diesel generators operation and the operation of the aggregate battery of the connected electric vehicles are jointly optimised for microgrid grid-connected and autonomous operation, satisfying a large number of technical, operational and environmental constraints of microgrid's operation.
- The proposed algorithm ensures the maximum possible reduction of the daily operation cost of the microgrid.
- The autonomous operation of the microgrid is ensured, mainly through the hosted PEVs and RES, reducing the need for investment to extra auxiliary power generation units.
- An efficient method to dispatch the total demand in thermal power of the microgrid to the thermal zones of the buildings according to their internal temperatures and volumes, is used.

To the best of the authors' knowledge and after a thorough review of the literature the features listed above are rarely found in similar systems and no other research work was found comprising and jointly applying them to microgrids of large-scale building prosumers.

2 | MAS STRUCTURE AND OPERATION

The operations of the microgrid are organised in a hierarchical MAS. MAS have been proved to be very efficient in the control and management of complex systems that might be difficult to attain by classical centralised control. They can also be effective for highly complex microgrids of large-scale building prosumers. The developed MAS comprises various categories of agents placed at different levels as shown in Figure 1. The agent operations are shown in Figure 2. Specifically, the examined energy system includes large-scale office buildings, large PEV parking lots, local power generators, PVs and wind turbines nearby the buildings. The loads of the examined microgrid can be supplied from its power sources and the main electric grid or only by the local power sources in island mode of operation, that is, diesel generators, RES and the hosted clusters of PEVs.

2.1 | Load agents

The agents Thermal Load Agent (TLA) and Electrical Load Agent (ELA) are associated with the buildings and placed at the first level of the MAS. They aim to model the thermal zone loads and building critical and non-critical electrical loads according to building specifications, occupancy, types of used appliances, conditioned space per thermal zone, outdoor temperature, solar radiation etc. Both thermal and non-critical electrical loads adjust their power within their operational and technical constraints. Another type of agent, Parking Dynamic Aggregate Battery Agent (PDABA), is placed on the lower level of the developed MAS and assigned with the development of an equivalent battery model for all PEVs of the microgrid. It collects the necessary data from the PEVs obtained by the processing of real-world data [26]. In this study,

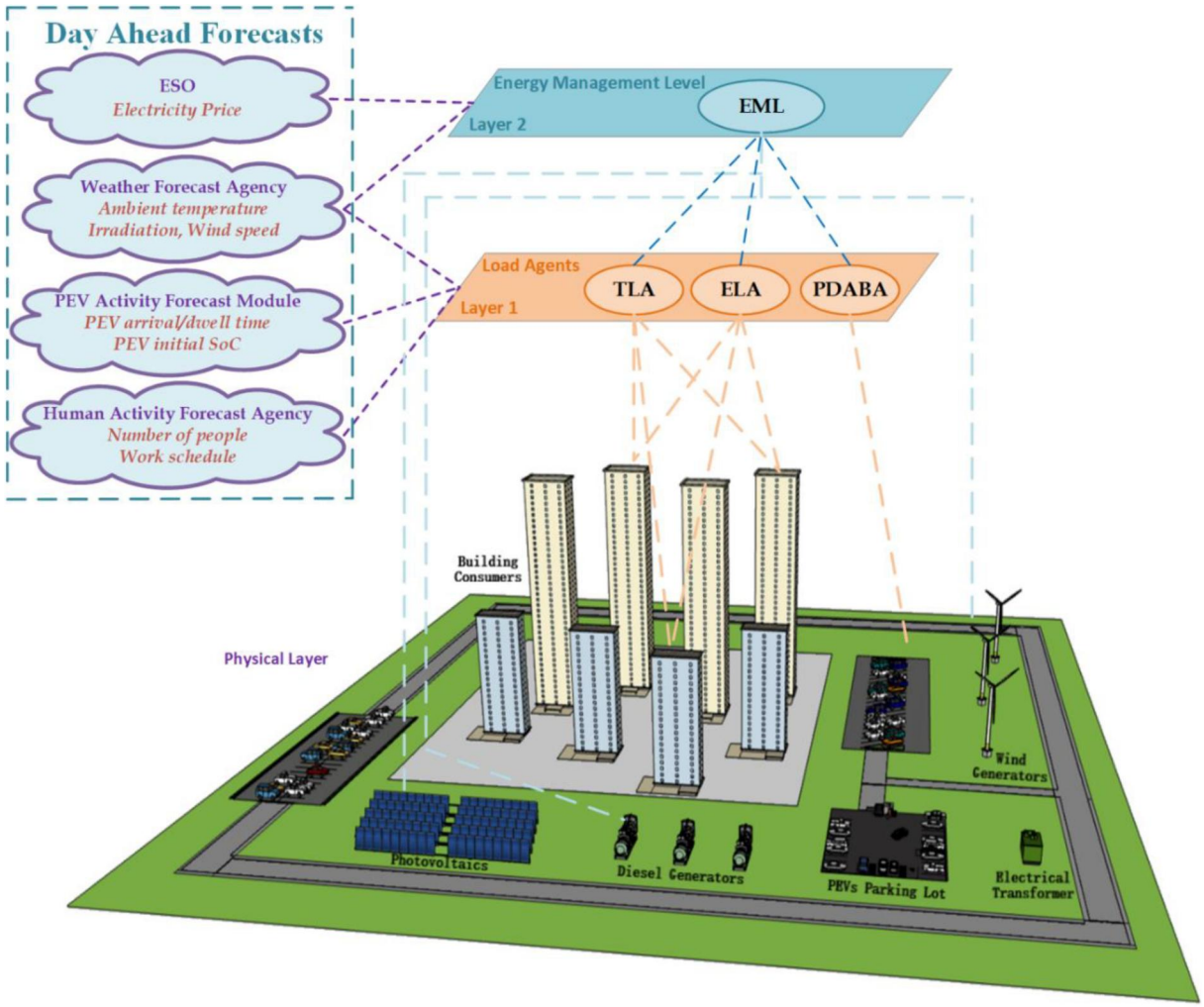

FIGURE 1 Configuration of the microgrid power management system.

PEVs comprise the V2G mode operation. TLA, ELA and PDABA are also responsible for the optimal dispatch of their power to the local agents they supervise and control.

2.2 | Energy management level

The main goal of MAS second level is the minimisation of the total daily operation cost of the microgrid on the assumption of operation under variable electricity price. It calculates the most effective operation schedule of the buildings' HVAC and electrical systems, PEV aggregator and local power generation units while a large number of constraints of the hosted PEVs, diesel generators and the building energy systems are satisfied. In addition, the reactive powers of the PEVs and building local power generators are suitably scheduled to maintain node voltages within their boundaries.

In order to minimise the computation time, the operation scheduling is performed at the highest possible level of integration, for example, microgrids of buildings and smart power dispatch techniques are applied to estimate the power set-points at component level, for example, thermal zones, PEVs etc. To achieve this, smart definitions of the flexibility of the microgrid components to change their power are performed and a new sub-optimisation problem that maximises the total flexibility of the system is solved to obtain the optimal power dispatch under all the associated constraints.

3 | MICROGRID COMPONENTS' MODEL

3.1 | Model of building thermal load agent

A thermal model for the HVAC system of each building thermal zone is constructed according to the equations shown below [27, 28]:

$$p \cdot C_z \cdot V_z \cdot \frac{dT_{in,z}}{dt} = \dot{Q}_{ex,wall,z} + \dot{Q}_{in,wall,z} + \dot{Q}_{win,z} + Q_{in,z} + \dot{Q}_{sw,z} + \dot{Q}_{sg,z} - Q_{EC,z} \quad (1)$$

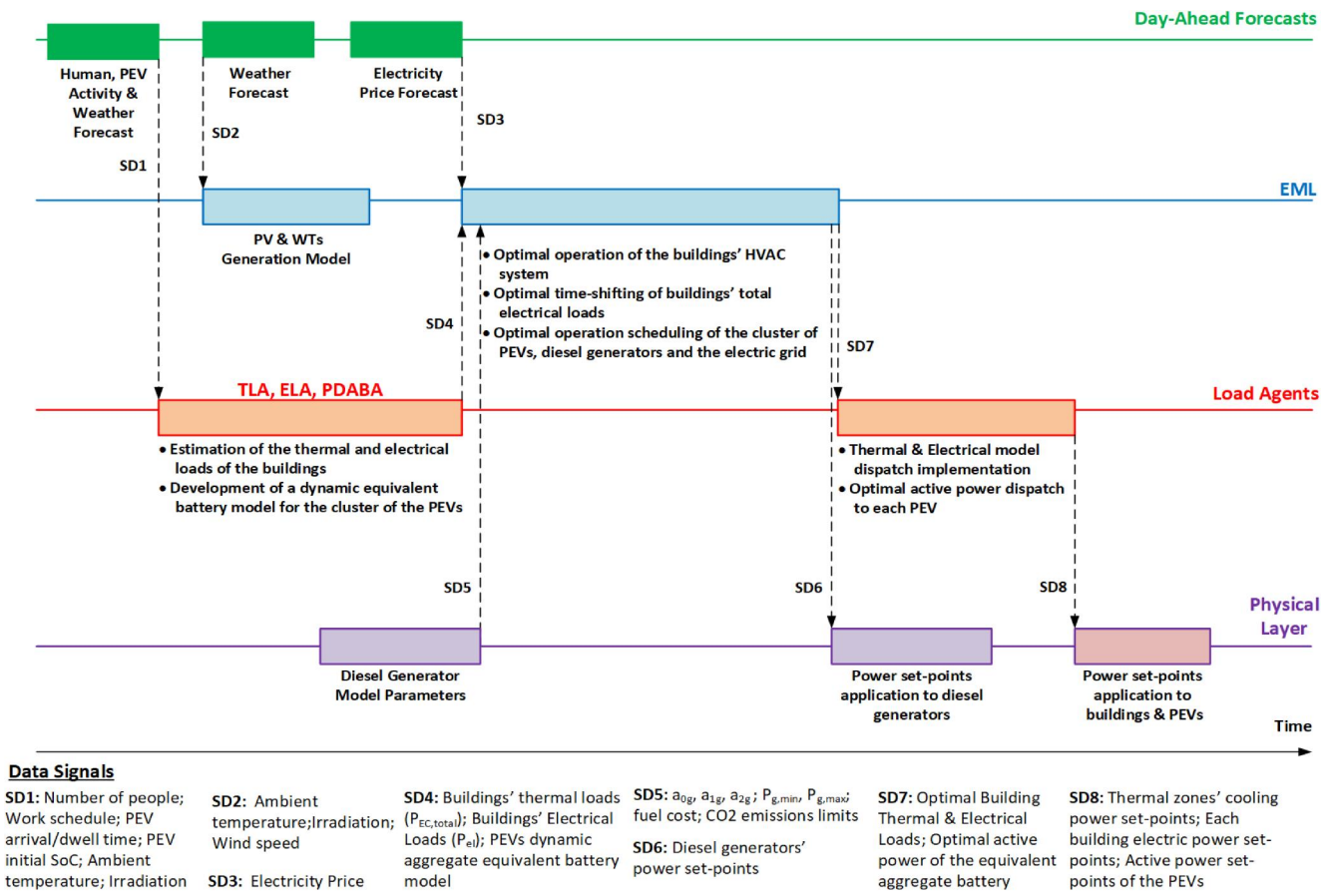

FIGURE 2 Communication signals sequence.

With,

$$\dot{Q}_{ex,wall,z} = \sum_{y\in\mathcal{E}} U_{wall,y} \cdot F_{wall,y} \cdot \left(T_{out} - T_{in,z}\right) \tag{2}$$

$$\dot{Q}_{win,z} = \sum_{y\in\mathcal{E}} U_{win,y} \cdot F_{win,y} \cdot \left(T_{out} - T_{in,z}\right) \tag{3}$$

$$\dot{Q}_{sw,z} = \sum_{y\in\mathcal{E}} a_w \cdot R_{se} \cdot U_{wall,y} \cdot F_{wall,y} \cdot I_{T,z} \tag{4}$$

$$\dot{Q}_{sg,z} = \sum_{y\in\mathcal{E}} \tau_{win} \cdot SC \cdot F_{win,y} \cdot I_{T,z} \tag{5}$$

$$\dot{Q}_{in,wall,z} = \sum_{y\in\mathcal{E}} U_{wall,y} \cdot F_{wall,y} \cdot \left(T_{in,nz} - T_{in,z}\right) \tag{6}$$

By appropriately modifying Equations (1)–(6), the state space system of equations is obtained for each building as follows:

$$\frac{d\boldsymbol{T_{in}}(t)}{dt} = \boldsymbol{A_b} \cdot \boldsymbol{T_{in}}(t) + \boldsymbol{B_b} \cdot \boldsymbol{U} \tag{7}$$

$$\boldsymbol{Y}(t) = \boldsymbol{C_b} \cdot \boldsymbol{T_{in}}(t) + \boldsymbol{D_b} \cdot \boldsymbol{U} \tag{8}$$

The input vector $\boldsymbol{U}$ is of dimension $(2N_Z + 2) \times 1$. It is given in Equation (9) as given below:

$$\boldsymbol{U} = \begin{bmatrix} Q_{EC,1}(t) \\ \vdots \\ Q_{EC,N_Z}(t) \\ Q_{in,1}(t) \\ \vdots \\ Q_{in,N_Z}(t) \\ T_{out}(t) \\ I_T(t) \end{bmatrix} \tag{9}$$

With

$$I_{T,z} = I_b \cdot R_b + I_d \cdot \left(\frac{1 + \cos\beta_z}{2}\right) + I \cdot p_g \cdot \left(\frac{1 - \cos\beta_z}{2}\right) \tag{10}$$

$$R_b = \frac{\cos\theta}{\cos\theta_z} \tag{11}$$

The elements of the matrix $\boldsymbol{A_b}$ with dimension $(N_Z \times N_Z)$ are calculated in Equations (12)–(13) as follows:

$$A_{j,j} = -\sum_{y\in\mathcal{E}} U_{wall,y}\cdot F_{wall,y} - \sum_{x\in\mathcal{J}} U_{wall,x}\cdot F_{wall,x} - \frac{1}{p\cdot C_z\cdot V_z}\cdot\sum_{y\in\mathcal{E}} U_{win,y}\cdot F_{win,y} \tag{12}$$

$$A_{j,i} = \begin{cases} \frac{1}{p\cdot C_z\cdot V_z}\cdot U_{wall,x}\cdot F_{wall,x}, & j,i\in\mathcal{N} \\ 0, & j,i\notin\mathcal{N} \end{cases} \tag{13}$$

The dimension of $\boldsymbol{B_b}$ is $N_Z\times(2N_Z+2)$ and it is calculated as given in the following equations:

$$\boldsymbol{B_b} = \frac{1}{p\cdot C_z\cdot V_z}\left[-\mathbf{I}_{(N_Z\times N_Z)} \quad \mathbf{I}_{(N_Z\times N_Z)} \quad \boldsymbol{B_{ex,w}} \quad \boldsymbol{B_{rad}}\right] \tag{14}$$

with

$$\boldsymbol{B_{ex,w}}_{(N_Z\times 1)} = \begin{bmatrix} B_{ex,w,1} \\ \vdots \\ B_{ex,w,N_Z} \end{bmatrix} \tag{15}$$

$$\boldsymbol{B_{rad}}_{(N_Z\times 1)} = \begin{bmatrix} B_{rad,1} \\ \vdots \\ B_{rad,N_Z} \end{bmatrix} \tag{16}$$

The elements of the submatrices $\boldsymbol{B_{ex,w}}$ and $\boldsymbol{B_{rad}}$ of matrix $\boldsymbol{B_b}$ are determined as follows.

$$B_{ex,w,z} = \sum_{y\in\mathcal{E}} U_{wall,y}\cdot F_{wall,y} + \sum_{y\in\mathcal{E}} U_{win,y}\cdot F_{win,y} \tag{17}$$

$$B_{rad,z} = \sum_{y\in\mathcal{E}} a_w\cdot R_{se}\cdot U_{wall,y}\cdot F_{wall,y} + \sum_{y\in\mathcal{E}} \tau_{win}\cdot SC\cdot F_{win,y} \tag{18}$$

Considering as output the internal temperatures of the thermal zones then the matrices $\boldsymbol{C_b}$ and $\boldsymbol{D_b}$ are defined as given in the following equations:

$$\boldsymbol{C_b}_{(N_Z\times N_Z)} = \mathbf{I}_{(N_Z\times N_Z)} \tag{19}$$

$$\boldsymbol{D_b}_{(N_Z\times 2N_Z+2)} = \mathbf{0}_{(N_Z\times 2N_Z+2)} \tag{20}$$

The system of continuous time Equations (7) and (8) is converted to discrete time Equations (21) and (22) as follows:

$$\boldsymbol{T_{in}}(k+1) = \boldsymbol{A_{b,d}}\cdot\boldsymbol{T_{in}}(k) + \boldsymbol{B_{b,d}}\cdot\boldsymbol{U} \tag{21}$$

$$\boldsymbol{Y}(k) = \boldsymbol{C_{b,d}}\cdot\boldsymbol{T_{in}}(k) + \boldsymbol{D_{b,d}}\cdot\boldsymbol{U} \tag{22}$$

3.2 | Model of building electrical load agent

Building's overall electric power consumption is calculated in Equation (23), as given below:

$$P_{el,b} = \sum_z P_{el_{load},z} \tag{23}$$

Where, $P_{el\_load,z}$ is the power consumption of the electrical loads of the zth thermal zone [29].

It is assumed that the non-critical electrical loads are defined by the rate n_{non_cr} as in Equation (24), as given below:

$$P_{non\_cr} = \sum_b n_{non\_cr}\cdot P_{el,b} \tag{24}$$

Let us assume that the window of time in which non-critical loads may be shifted is $\left[\mathrm{T}_{shift,0}\ \mathrm{T}_{shift,f}\right]$ then the non-critical loads are optimally adjusted in Equations (25)–(27), asgivenbelow:

$$P^*_{non\_cr}(t) = \begin{cases} n_{shift}(t)\cdot P_{non\_cr}(t), & \forall t\in\left[\mathrm{T}_{shift,0}\ \mathrm{T}_{shift,f}\right] \\ P_{non\_cr}(t), & otherwise \end{cases} \tag{25}$$

$$n_{shift,min} \le n_{shift} \le n_{shift,max} \tag{26}$$

$$\sum_{t=\mathrm{T}_{shift,0}}^{\mathrm{T}_{shift,f}} P_{non\_cr}(t)\cdot\Delta t = \sum_{t=\mathrm{T}_{shift,0}}^{\mathrm{T}_{shift,f}} P^*_{non\_cr}(t)\cdot\Delta t \tag{27}$$

3.3 | Parking dynamic aggregate battery agent

An aggregate battery model for the PEVs is described next. It is derived using predictions of PEVs' plug-in and dwell times, charge levels at plug-in time, and battery technical specifications as described in Ref. [28, 30]. Equations (28)–(31) are used to estimate the time-varying maximum and minimum limits of the power and store energy of the equivalent battery.

$$P_{PB,max}(t) = \sum_i P_{max}(i,t) \tag{28}$$

$$P_{PB,min}(t) = \sum_i P_{min}(i,t) \tag{29}$$

$$SoC_{PB,max}(t) = \sum_i SoC_{high}(i,t) - SoC_{diff}(t) \tag{30}$$

$$SoC_{PB,min}(t) = \sum_i SoC_{low}(i,t) - SoC_{diff}(t) \tag{31}$$

The continuous plugging and unplugging of electric vehicles cause a continuous change of the stored energy of the

aggregate battery which is represented by SoC_{diff} and is calculated in Equations (32)–(34).

$$SoC_{diff}(t) = \sum_{T_0:\Delta t:t} \left(SoC_{0,PB}(t) - SoC_{t,PB}(t)\right) \quad (32)$$

$$SoC_{0,PB}(t) = \sum_{\forall ith\ EV\ plugged\ at\ t} SoC_0(i) \quad (33)$$

$$SoC_{t,PB}(t) = \sum_{\forall ith\ EV\ unplugged\ at\ t} SoC_{target}(i) \quad (34)$$

Let us assume that the optimal active power the equivalent battery exchanges with the electric grid is $P_{opt}(t)$ and generator convention is used then the SoC (in kWh) is calculated according to Equation (35).

$$SoC_{PB}(t+\Delta t) = \begin{cases} SoC_{PB}(t) - P_{opt}(t)\cdot n_{ch}\cdot \Delta t, & P_{opt}(t) < 0 \\ SoC_{PB}(t) - \dfrac{P_{opt}(t)}{n_{disch}}\cdot \Delta t, & P_{opt}(t) \geq 0 \end{cases} \quad (35)$$

The following constraints Equations (36)–(38) should be satisfied by the equivalent aggregate battery.

$$SoC_{PB}(T_0) = SoC_{PB}(T_f) \quad (36)$$

$$SoC_{PB,min}(t) \leq SoC_{PB}(t) \leq SoC_{PB,max}(t) \quad \forall\, t \in \left[T_0\ T_f\right] \quad (37)$$

$$P_{PB,min}(t) \leq P_{opt}(t) \leq P_{PB,max}(t) \quad \forall\, t \in \left[T_0\ T_f\right] \quad (38)$$

3.4 | Operation scheduling of diesel generator set

The fuel cost of the gth diesel generator at time t is estimated as follows [28, 31]:

$$FC_g\left(P_g(t)\right) = a_{0g} + a_{1g}\cdot P_g(t) + a_{2g}\cdot P_g(t)^2 \quad (39)$$

The fuel consumption function (kgFuel/h) of the gth generator is as given below:

$$FuelCon\left(P_g(t)\right) = \frac{FC_g\left(P_g(t)\right)}{FuelCost_g} \quad (40)$$

Where, $FuelCost_g$ is the cost of the fuel consumed by the gth generator (m.u./kgFuel).

The mass of the gas emissions of the g th generator produced in time interval Δt is calculated as given in the following equation:

$$m_{em,g}\left(P_g(t)\right) = c_{em,g}\cdot FuelCon\left(P_g(t)\right)\cdot \Delta t \quad (41)$$

where $m_{em,g}$ (in $kgEm_g/h$) is the mass of the g th diesel generator pollutant emission and $c_{em,g}$ (in $kgEm_g/kgFuel$) is the conversion factor of fuel mass to emission mass Em_g.

Let us consider that st_g denotes the state of operation of the gth generator (if the gth generator operated then $st_g = 1$ otherwise $st_g = 0$) then the minimum operation cost of the diesel generators at time t is obtained by solving the optimisation problem in Equations (42)–(46).

$$TC(t) = \min_{st_g, P_g} \sum_{g\in\mathcal{G}} \left(st_g(t)\cdot FC_g\left(P_g(t)\right)\right)\cdot \Delta t \quad (42)$$

S.t.

$$st_g(t)\cdot P_{g,min} \leq P_g(t) \leq st_g(t)\cdot P_{g,max}, \forall t, g \quad (43)$$

$$t_{OFF,g} - t_{ON,g} \geq T_{ON\_min,g}, \forall g \quad (44)$$

$$t_{ON,g} - t_{OFF,g} \geq T_{OFF\_min,g}, \forall g \quad (45)$$

$$st_g(t)\cdot m_{em,g}(t) \leq limEm_g, \forall g \quad (46)$$

Where, $limEm_g$ (in kg/h) denotes the emissions upper limit of the gth diesel generator. Minimum allowed duration of generator continuous operation or not ensured by Equations (44) and (45), respectively.

3.5 | Distribution network

Let us consider that the state of operation of the microgrid is denoted with the variable st_{grid} and the microgrid operates autonomously for $t \in \left[T_{auto,0}\ T_{auto,f}\right]$.

The power balance between the electric network and the microgrid of building prosumers is ensured by the following constraint,

$$\begin{aligned} &P_{EC,total}(t) + P_{el}(t) + P_{DNload}(t) \\ &= st_{grid}(t)\cdot P_{grid}(t) + P_{opt}(t) + P_{PV}(t) \\ &\quad + P_{WT}(t) + \sum_{g\in\mathcal{G}} st_g(t)\cdot P_g(t)\Big) \end{aligned} \quad (47)$$

With,

$$st_{grid}(t) = \begin{cases} 0, & \forall t \in \left[T_{auto,0}\ T_{auto,f}\right] \\ 1, & otherwise \end{cases} \quad (48)$$

The building diesel-generators and the PEVs' parking lot are able to regulate their reactive power according to a specific V-Q droop curve. Let us consider that $Q(t)$, $Q_g(t)$ denote the output reactive power of the PEVs' parking lot and the gth diesel generator at time t. Then they can be calculated as given in the following equations:

$$Q_g(t) = -R_{v,dg} \cdot V_{dg} + b_{v,dg}, Q_{g,min} \le Q_g(t) \le Q_{g,max} \quad (49)$$

$$Q_{PEV}(t) = -R_{v,PEV} \cdot V_{PEV} + b_{v,PEV}, Q_{PEV,min} \le Q_{PEV}(t) \le Q_{PEV,max} \quad (50)$$

Where, $R_{v,dg}$, $R_{v,PEV}$ are the voltage droops of the diesel generators and the parking lot of PEVs, V_{dg} and V_{PEV} denote voltage amplitude at the nodes the diesel generators and the PEV parking lot are connected, respectively. $b_{v,dg}$ and $b_{v,PEV}$ are constants defined by the operator of the microgrid.

Let us assume that $\boldsymbol{V}, \boldsymbol{\theta}$ are the voltage and angle vectors of distribution network voltages, $\boldsymbol{P}$, $\boldsymbol{Q}$ are vectors comprising the active and reactive powers injected to network nodes and ε is a small positive real number then the iterative process described by the following pseudocode in Algorithm 1 is applied to determine the state of operation of the electric network of the microgrid given that the reactive powers of the PEV's parking lot and building auxiliary generators are regulated according to Equations (49), (50).

Algorithm 1 Pseudocode to determine the state operation of the electric network.

Initialize voltage and angle vectors to $\boldsymbol{V}(1), \boldsymbol{\theta}(1)$
$k = 1$; $e(1) = 5\varepsilon$;
While $e(k) > \varepsilon$
Do
$k = k + 1$;
$Q_g(k) = -R_{v,dg} \cdot V_{dg}(k-1) + b_{v,dg}, Q_{PEV}(k)$
$= -R_{v,PEV} \cdot V_{PEV}(k-1) + b_{v,PEV}$;
$[\boldsymbol{V}(k), \boldsymbol{\theta}(k)] = PowerFlow(\boldsymbol{V}(k-1), \boldsymbol{P}, \boldsymbol{Q})$;
$e(k) = (\boldsymbol{V}(k) - \boldsymbol{V}(k-1))^T \cdot (\boldsymbol{V}(k) - \boldsymbol{V}(k-1))$;
end

3.6 | Model of wind power generation estimation

The electric power generation estimation of the WTs of the microgrid is provided in Equation (51).

$$\widehat{P}_{WT} = \begin{cases} 0, & V_{cut,off} < \widehat{V} < V_{cut,in} \\ P_{WT,nom} \cdot \dfrac{\widehat{V}^3 - V_{cut,in}^3}{V_N^3 - V_{cut,in}^3}, & V_{cut,in} \le \widehat{V} < V_{nom} \\ P_{WT,nom}, & V_{nom} \le \widehat{V} < V_{cut,off} \end{cases} \quad (51)$$

Where $P_{WT,nom}$ is the nominal electric power of the WTs, $\widehat{V}$ is the forecasted wind velocity, V_{nom} is the nominal wind velocity of the WTs and $V_{cut,in}$ ($V_{cut,off}$) is the cut-in (cut-off) wind velocity.

3.7 | Model of photovoltaic power generation estimation

The electric power generation estimation of the PVs of the microgrid is provided in Equation (52).

$$\widehat{P}_{PV} = n_{PV} \cdot P_{PV,nom} \cdot \frac{\widehat{G}}{G_{ref}} \cdot \left[1 + K_t\left(\left(\widehat{T}_{out} + 0.0256 \cdot \widehat{G}\right) - T_{ref}\right)\right] \quad (52)$$

Where n_{PV} is the performance coefficient of the PV power converter, $P_{PV,nom}$ is the nominal power of the PV generator, $\widehat{G}$ is the forecasted solar radiation, G_{ref} is the reference solar radiation equal to $1000 W/m^2$, T_{ref} is the panel temperature in standard test conditions equal to 25℃ and K_t is a constant equal to $-0.0357\,°C^{-1}$.

4 | OPTIMAL OPERATION SCHEDULING OF THE MICROGRID

EML agent uses Particle Swarm Optimisation (PSO) and applies it at microgrid scale to facilitate the optimisation process. PSO is one of the most highly efficient heuristic methods and its implementation is remarkably simple. PSO has proved very robust and efficient for application to complex optimisation problems as it does not depend on the selected initial point and leads to a global optimum with a high rate of success. It is difficult to find the global optimum for large-dimension optimisation problems and formulate extremely complex objective functions using classical methods. In the examined problem, the building thermal model's differential equations, PEVs aggregated model and distribution network model should be solved within the optimisation procedure, making its implementation difficult if classical optimisation techniques are applied. However, using PSO algorithm, this problem is overcome since the objective function can be arbitrarily complex and of any form. It can also be easily adjusted in case that new components need to be included. Specifically, EML provides the optimal total electric power demand of the HVAC systems and optimally shifts building non-critical electrical loads with the purpose of minimising the building's total daily energy demand and cost. Moreover, the charging of the hosted PEVs and the operation of the local power generation units is optimally scheduled. The structure of each particle of the swarm with its different parts comprising the respective decision variables associated with the optimisation of the aforementioned microgrid subsystems is given in Figure 3.

Some more information about the particle part concerning building generators optimisation is provided next. Let us assume that N_g is the number of the diesel generators. Each dimension in this particle part contains a number, S, that takes values from 0 to $2^{N_g} - 1$ and corresponds to the state of operation of the diesel generators set. This number is

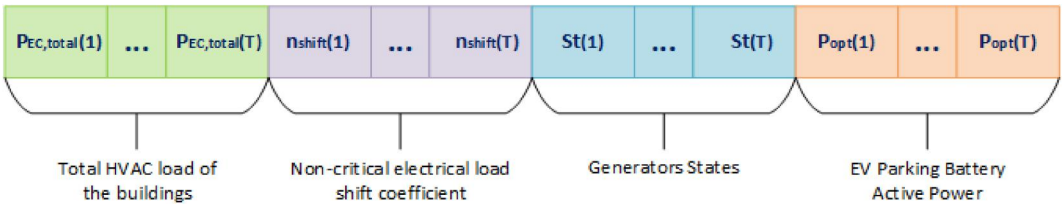

FIGURE 3 Particle structure used by the EML.

transformed to binary number containing the state of operation of each diesel generator as described in Equation (53).

$$\left[st_1(t)\ldots st_{Ng}(t)\right] = \boldsymbol{dec2bin}\left(round(S(t)), S \in \left[0 \quad 2^{Ng}-1\right]\right) \tag{53}$$

Where, $\boldsymbol{dec2bin}(round(N(t))$ represents the conversion function of a decimal number to binary.

The augmented cost function used by the PSO including the applied constraints, are given in Equation (54). The goal of the optimisation process is the minimisation of the total daily operation cost of the microgrid according to the electricity price and the satisfaction of all microgrid's components constraints integrated in term (Pen) of the objective function.

$$TC_{MG} = \min_{\substack{st_g, P_{grid}, P_{opt}, \\ P_{EC,total}, n_{shift}}} \left\{ \left(\sum_t P_{grid}(t) \cdot EP(t) + \sum_t \sum_{g \in \mathcal{G}} st_g(t) \cdot FC_g\left(P_g(t)\right) \right) \cdot \Delta t + Pen \right\} \tag{54}$$

S.t. Equations (25)–(27), (36)–(38), (43)–(47).

Sub-optimisation problems are solved in order to optimally dispatch: (a) the total thermal power to each building thermal zone, (b) the total power consumed by all microgrid building electrical loads to each building and (c) the active power consumed/produced by PEVs aggregator to each separate PEV. To this end, suitable flexibility indices are developed for each type of microgrid component.

4.1 | Optimal power dispatch algorithm

Considering a summer cooling scenario, the thermal model dispatch is implemented as formulated in Equation (55)–(59).

$$Q_{EC,z}(t) = \frac{\frac{T_{in,z}(t)-T_{min,z}}{T_{max,z}-T_{min,z}} \cdot V_z}{\sum_z \left\{ \frac{T_{in,z}(t)-T_{min,z}}{T_{max,z}-T_{min,z}} \cdot V_z \right\}} \cdot Q_{EC,total}(t) \tag{55}$$

$$T_{min,z} \le T_{in,z}(t) \le T_{max,z} \tag{56}$$

$$P_{EC,total,min} \le P_{EC,total}(t) \le P_{EC,total,max} \tag{57}$$

$$P_{EC,total,min,b} \le P_{EC,total,b}(t) \le P_{EC,total,max,b}, \quad \forall b \in B \tag{58}$$

$$\sum_b P_{EC,total,b}(t) = P_{EC,total}(t) \tag{59}$$

$$P_{EC,z} = \frac{Q_{EC,z}}{COP}, P_{EC,total} = \frac{Q_{EC,total}}{COP} \tag{60}$$

If any of the technical limits of the HVAC consumption of a building is violated, the total power of this building is set equal to the technical limit violated ($P'(t)$), and then subtracted from the total cooling power consumed by all microgrid's buildings ($P_{new}(t) = P_{EC,total}(t) - P'(t)$). The dispatch of the total thermal power consumption is reapplied and the total power P_{new} is dispatched to each thermal zone of the other buildings.

An optimisation problem is solved in order to optimally dispatch the total power consumed by the buildings' electrical loads of the microgrid to each individual building, while satisfying all the technical and operational constraints. The augmented objective function is given below in Equation (61):

$$\min_{n^*_{shift,b}} \left\{ \sum_t \left(\sum_{b \in B} \left(n^*_{shift,b}(t) - n_{shift}(t) \right)^2 \right) \right\} \tag{61}$$

S.t.

$$\sum_{t=\mathrm{T}_{shift,0}}^{\mathrm{T}_{shift,f}} P_{el,non,b}(t) \cdot \Delta t = \sum_{t=\mathrm{T}_{shift,0}}^{\mathrm{T}_{shift,f}} P^*_{el,non,b}(t) \cdot \Delta t, \quad \forall b \in B \tag{62}$$

$$\sum_{b \in B} P^*_{el,non,b}(t) = P^*_{non_{cr}}(t) \tag{63}$$

with

$$P^*_{el,non,b}(t) = \begin{cases} n^*_{shift,b}(t) \cdot P_{el,non,b}(t), & \forall t \in \left[\mathrm{T}_{shift,0} \ \ \mathrm{T}_{shift,f}\right] \\ P_{el,non,b}(t), & otherwise \end{cases} \tag{64}$$

Where, $n^*_{shift,b}$ is the load shifting coefficient and $P^*_{el,non,b}$ is the optimal electric power consumption by the non-critical loads of *bth* building of the microgrid.

A last optimisation problem is solved to optimally share the active power of the microgrid's parking lot to the PEVs

with target to maximise the sum of PEV flexibilities and satisfy all PEVs' constraints. The flexibility of a PEV to change its active power is defined in Ref. [32] and also followed in the present work. The used augmented objective function is given below in Equation (65):

$$\max_{P^*_{PEV}(i,t)} \sum_i flex_{PEV}(i, t + \Delta t) \tag{65}$$

S.t.

$$P^*_{PEV}(i,t) \le P_{max}(i), \forall i \tag{66}$$

$$P^*_{PEV}(i,t) \ge P_{min}(i), \forall i \tag{67}$$

$$SoC_{PEV}(i,t) - P^*_{PEV}(i,t) \cdot \Delta t < SoC_{high}(i, t + \Delta t), \forall i \tag{68}$$

$$SoC_{PEV}(i,t) - P^*_{PEV}(i,t) \cdot \Delta t > SoC_{low}(i, t + \Delta t), \forall i \tag{69}$$

$$\sum_i P^*_{PEV}(i,t) = P_{opt}(t) \tag{70}$$

Constraints Equations (68) and (69) ensure that $SoC(i,t)$ is maintained within permissible operation limits and allow each PEV reach the target of stored energy at its disconnection time.

5 | CASE STUDY

The developed models and algorithms are verified through the simulation of realistic microgrid operation scenarios. A notable feature of this work is that the developed methods are fully parametric in order to ensure the application of the finally developed energy management to energy systems of various sizes and complexity. Particularly, the proposed energy system is able to include buildings scaling from simple residential ones up to mega office or commercial buildings, buildings with simple floor plans and a few thermal zones up to buildings with complex floor plans and large number of thermal zones. This is achieved by appropriately modifying model parameters, such as the number of thermal zones and building floors, the buildings' dimensions and construction characteristics, the profiles of building thermal and electrical loads for each building thermal zone.

In this work we have chosen to examine large-scale office buildings which are more challenging to optimise due to their complexity. Moreover, in the examined case study, three kinds of floor plans are selected for demonstration purposes in order to examine and compare the thermal behavior of buildings with different characteristics and complexity, as shown in Figure 4. In our case study, theoretically the decision variables amount up to 57,220. The single-line of the examined IEEE 33-node electric distribution network is shown in Figure 5. Tables 1 and 2 include the necessary buildings' model

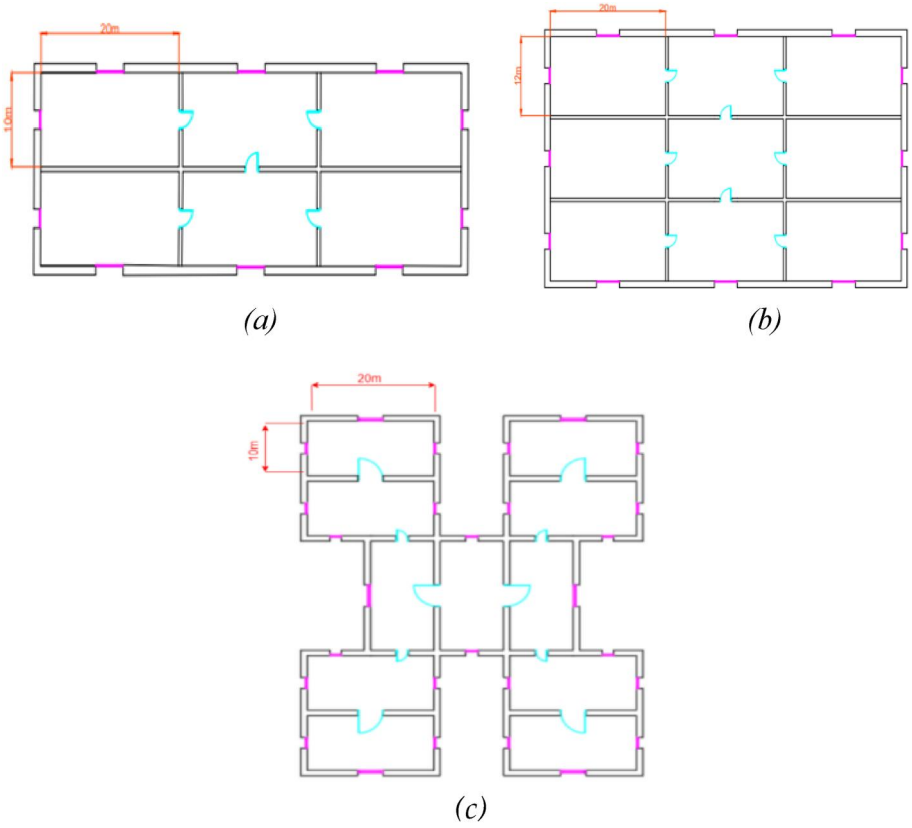

FIGURE 4 Floor plans (a) Building 1 (20 floors, 120 thermal zones), (b) Building 2 (40 floors, 360 thermal zones), and (c) Building 3 (70 floors, 770 thermal zones).

parameter data. Finally, Table 3 provides the technical specifications of building diesel generators.

Three representative operation scenarios (OSC) of the examined microgrid were simulated in this study. They are briefly described next and the major respective information is tabulated in Table 4.

(1) OSC I

In this scenario, the goal is to minimise the overall operation cost of the microgrid.

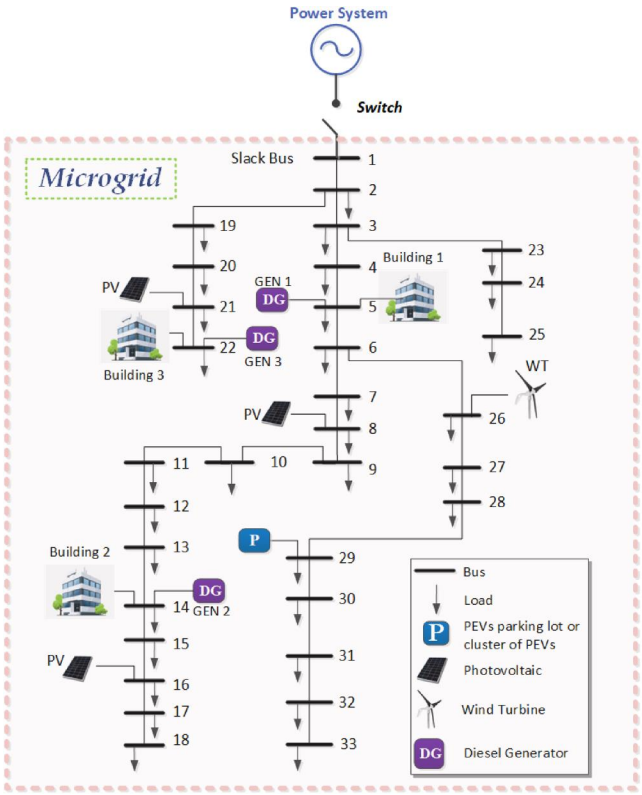

FIGURE 5 Single-line diagram of microgrid electric network.

(2) OSC II

In OSC II, in addition to the OSCI microgrid autonomous operation is also included. It is assumed that a grid power supply interruption occurs during 15:00 p.m.–18:00 p.m. and the microgrid should cover its total electric power demand using only its available resources. Specifically, the EV parking lot, renewable energy sources and the diesel generators should supply the building and distribution network loads.

(3) OSC III

In OSC III, no optimisation technique is applied to the operation of building thermal and electric power systems and the operation of PEV parking lot is not optimised, too. One goal is to keep the indoor temperature of all thermal zones of the buildings close to a constant value. For a fair comparison between the two operation scenarios, this temperature set point is set to the median indoor temperature obtained in OSC I. OSCIII represents the business-as-usual scenario of the microgrid and is used to estimate the overall operation cost reduction of the microgrid obtained by the suggested energy management strategy.

All the indoor temperatures of the thermal zones of the microgrid buildings are maintained at a fixed predefined temperature value using a PI controller as shown in Equations (71)–(72):

TABLE 2 Non-critical loads data

	Building 1	Building 2	Building 3
n_{non_cr}	0.25	0.25	0.25
$n_{shift,min}$	0.70	0.75	0.65
$n_{shift,max}$	1.3	1.25	1.25
$T_{shift,min}$	07:00	07:00	07:00
$T_{shift,max}$	17:00	17:00	17:00

TABLE 1 Building model data

Thermal zones modelling data									
	Thermal zones								
	Building 1	**Building 2**	**Building 3**	**All thermal zones**					
Side_1 (m)	10	12	10	$\rho(\mathrm{kg/m^3})$	1.2	$\tau_{win,z}$	$1.1 \cdot 10^{-3}$	$\beta_z(^\circ)$	90
Side_2 (m)	20	20	20	$C_z(\mathrm{kWh/(kg \bullet ^\circ C)})$	1/3600	$a_{w,z}$	$18.6 \cdot 10^{-3}$	$\theta(^\circ)$	11.9
Height (m)	3	3	3	$U_{wall,z}(\mathrm{kW/(m^2 \bullet ^\circ C)})$	$2.04 \cdot 10^{-3}$	SC_z	0.54	$\theta_z(^\circ)$	39.9
T_{min}/T_{max} (°C)	19/27.5	19/27.5	19/27.5	$U_{win,z}(\mathrm{kW/(m^2 \bullet ^\circ C)})$	$5.6 \cdot 10^{-3}$	p_g	0.2	$R_{se,z}(\mathrm{(m^2 \bullet ^\circ C)/kW})$	40
Building parameters									
				Building 1		**Building 2**			**Building 3**
Number of floors				20		40			70
Total number of thermal zones				120		360			770

TABLE 3 Building auxiliary generators data

Diesel generators parameters			
	G1	**G2**	**G3**
Technical minimum (kW)	285	620	1226
Technical maximum (kW)	1000	2170	4300
Minimum hours for generator being in operation/out of operation (h)	1/1	1/1	1/1

TABLE 4 Operation scenarios

Operation Scenario	I	II	III
HVAC optimisation	√	√	-
Electrical loads optimisation	√	√	-
Electric vehicles optimisation	√	√	-
Diesel generators optimisation	√	√	√
Renewable energy sources	√	√	√
Microgrid islanded operation	-	√	-
Total operation cost (m.u.)	25261	26965	32280

$$Q_{EC,z}(t) = K_P \cdot e(t) + K_I \cdot \int e(t) \cdot dt \tag{71}$$

$$e(t) = T_{in,z}(t) - T_{ref} \tag{72}$$

Moreover, PEVs are assumed to operate in 'dump' charging mode in OSC III. More specifically, they charge their batteries by absorbing the required constant quantity of power from the main electric grid that is estimated in Equation (73).

$$P_{dump}(i) = \frac{SoC_0(i) - SoC_{target}(i)}{t_f(i) - t_0(i)} \tag{73}$$

Figure 6a depicts the outdoor temperature while electricity price time series is shown in Figure 6b. Figure 7a depicts the number of occupants being in each building over time. The total power consumption of the distribution network loads, PV and WT power generations are shown in Figure 7b.

The probability density functions (PDFs) depicted in Figure 8a,b are used to estimate the arrival and dwell times of the electric vehicles. Figure 9 depicts the total number of PEVs over time.

Figure 10a,b depict the indoor temperatures of all building thermal zones for OSC I and OSC III, respectively. It is shown

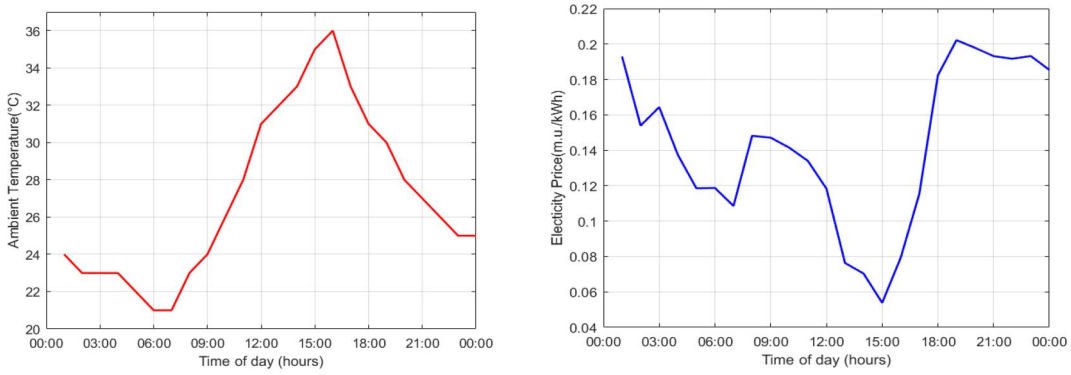

FIGURE 6 (a) Outdoor temperature (b) Variable electricity price.

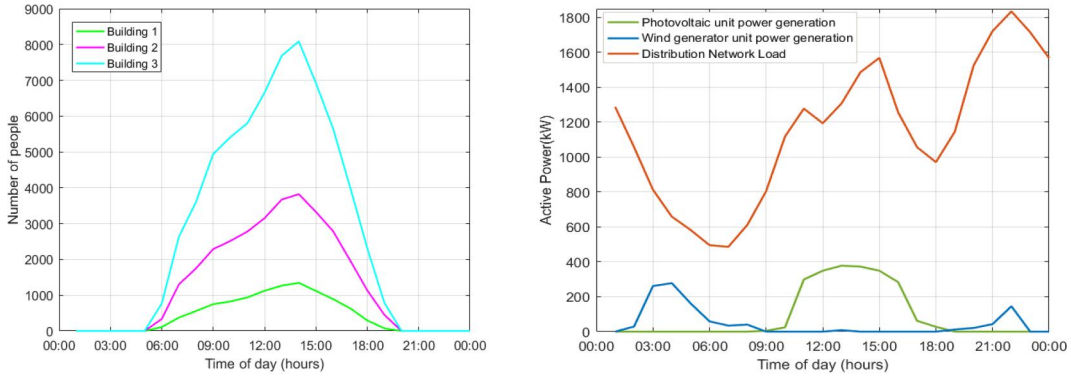

FIGURE 7 (a) Forecasted number of occupants (b) Distribution network load, PV and WT.

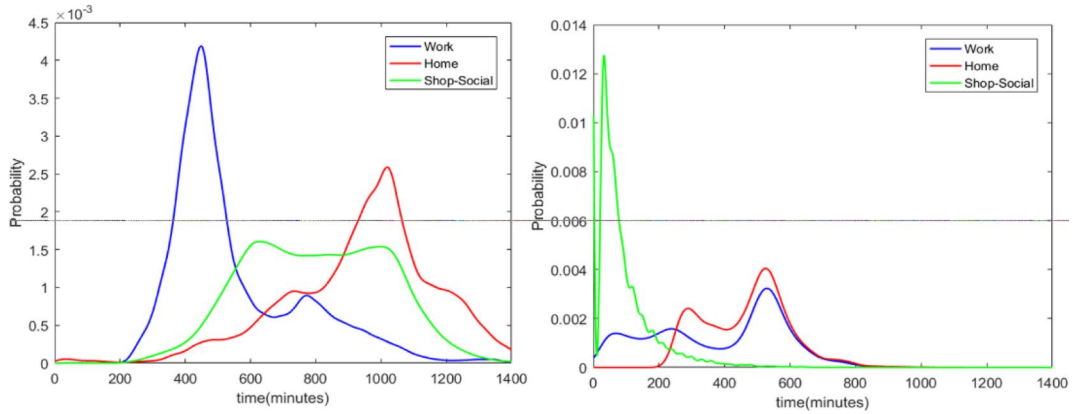

FIGURE 8 (a) PDF of PEV arrival time and (b) PDF of PEV dwell time.

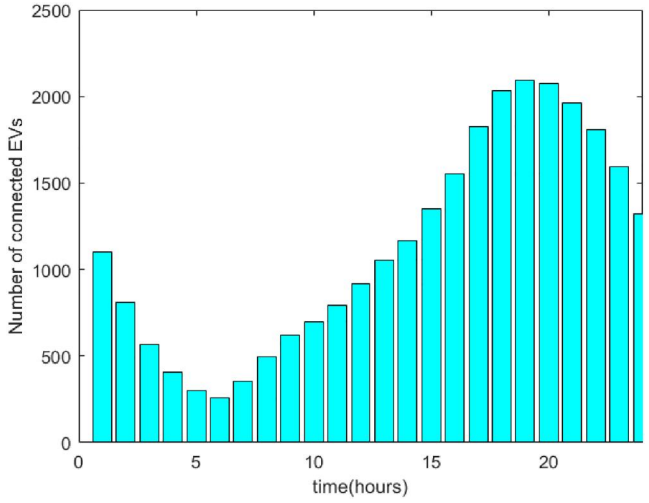

FIGURE 9 Number of connected PEVs.

that in OSC I, where the proposed optimisation method is applied, all indoor temperatures are kept within the desired temperature limits set by the occupants, they vary over time and they tend to behave in a similar way. In OSC III, the indoor temperatures are stabilised near to a predefined constant value.

The total electric power cooling demand of the HVAC systems for OSC I (the same with OSC II) and OSC III are shown in Figure 11a. The electric power consumption for each building thermal needs is strongly affected by the ambient temperature and the number of occupants in the offices. Moreover, in OSC I, the algorithm increases the total cooling requirements of the building prosumers when the electricity price takes its minimum value provided that temperature constraints allow it.

Figure 11b exhibits the total power of the buildings' non-critical loads obtained in OSC I before and after being optimised. It is verified through the plots that the suggested algorithm aims to suitably shift in time the consumption of non-critical loads to reduce the operation cost.

Figure 12a,b depict the active power and the total energy of the aggregate battery of the PEVs together with their bounds for all examined scenarios. In OSC I, the equivalent battery of the PEVs absorbs power from the utility grid or injects power according to the variable electricity price in order to contribute to the minimisation of the microgrid's overall operation cost. In OSC II, during autonomous operation, the aggregate battery of the PEVs is mainly used to meet the energy needs of the microgrid providing the necessary amount of energy to it. In OSC III, PEVs are not subject to any optimisation process and as it can be seen in the respective figures they only absorb the necessary amount of power from the grid in order to charge their batteries.

The power produced by the diesel generators is shown in stack form in Figure 13a for OSC II. Each generator is adjusted to operate as close as possible to its optimal operation point during the examined time period. In Figure 13b, CO_2 emissions of each diesel generator of the microgrid are shown for OSC II. The algorithm maintains the pollutant emissions of all auxiliary generators below their limits (only the third diesel generator was forced to limit its emissions).

The power at the microgrid grid coupling point is given in Figure 14 for the OSCI-OSCIII. It is observed that in OSC I, the electric power grid supplies the microgrid with large amounts of power during the time period when the electricity price is low, while the opposite happens when the electricity price is high. Moreover, it can be seen that the electric power grid does not exchange power with the microgrid during 15:00–18:00 in OSC II as the microgrid is in island operation during this time period.

Node voltages are shown in Figure 15a,b for OSC I and II, respectively. Voltage boundaries were set to 1.1 and 0.9 p.u. In both scenarios, the voltages of the network buses are well maintained within the predefined limits.

The operation cost of the microgrid obtained for examined operation scenarios are shown in Table 4. The obtained results indicate that the total daily microgrid's operation cost can be significantly reduced by the proposed method, in the range of 27%, with regard to the business-as-usual operation scenario. It is acknowledged that the buildings and the microgrid could have conflicted interests regarding the operation cost savings. To this end and for the sake of fairness, the total profit of the microgrid can be optimally and fairly allocated to the building

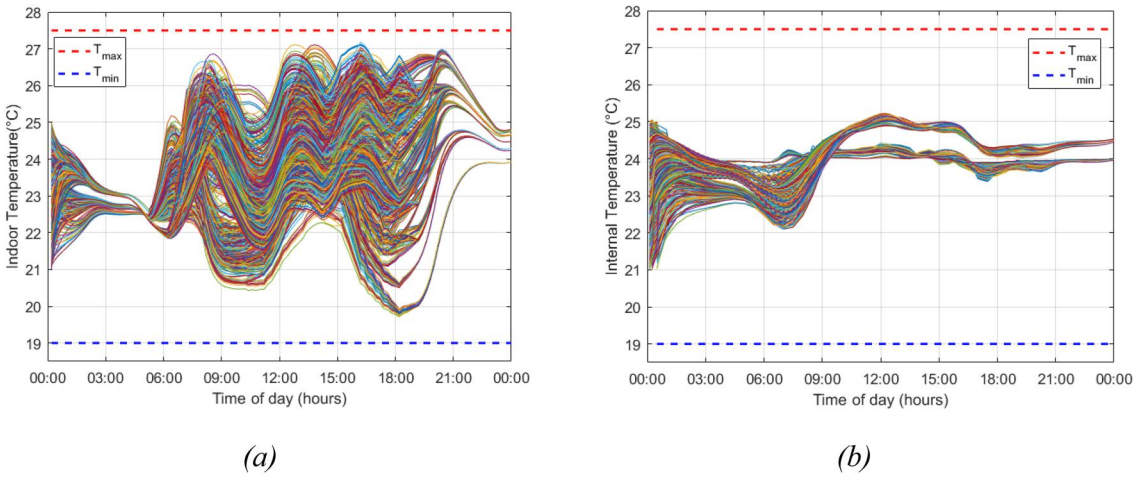

FIGURE 10 Internal temperatures of all thermal zones (a) (OSC I and II) and (b) (OSC III).

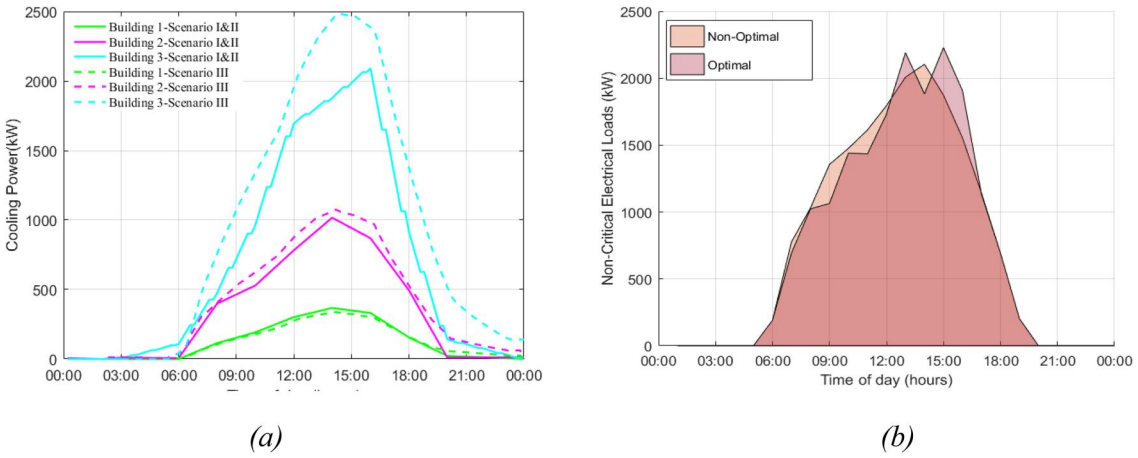

FIGURE 11 (a) Electric cooling power (OSC I and III) and (b) non-critical electrical loads before and after optimisation.

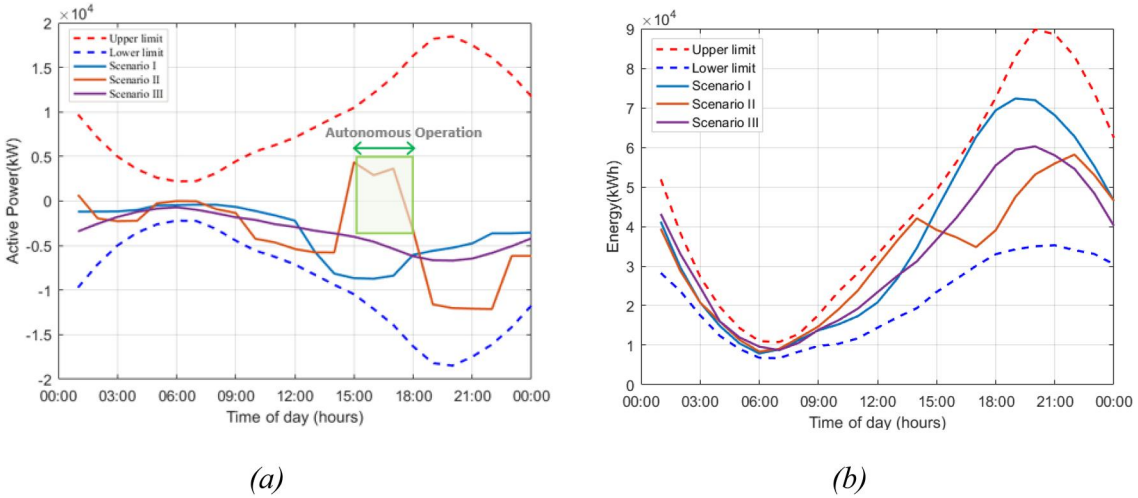

FIGURE 12 (a) Active power and (b) energy stored of EV aggregate battery with their respective limits (OSC I, II and III).

prosumers and plug-in electric vehicles hosted by the microgrid by developing suitable optimisation algorithms. A cost increase of 1704 m.u./day between OSC I and II is obtained due to the fact that the microgrid is forced to operate autonomously in OSC II during 15:00–18:00 while the electricity price happens to be the lowest values within this time period.

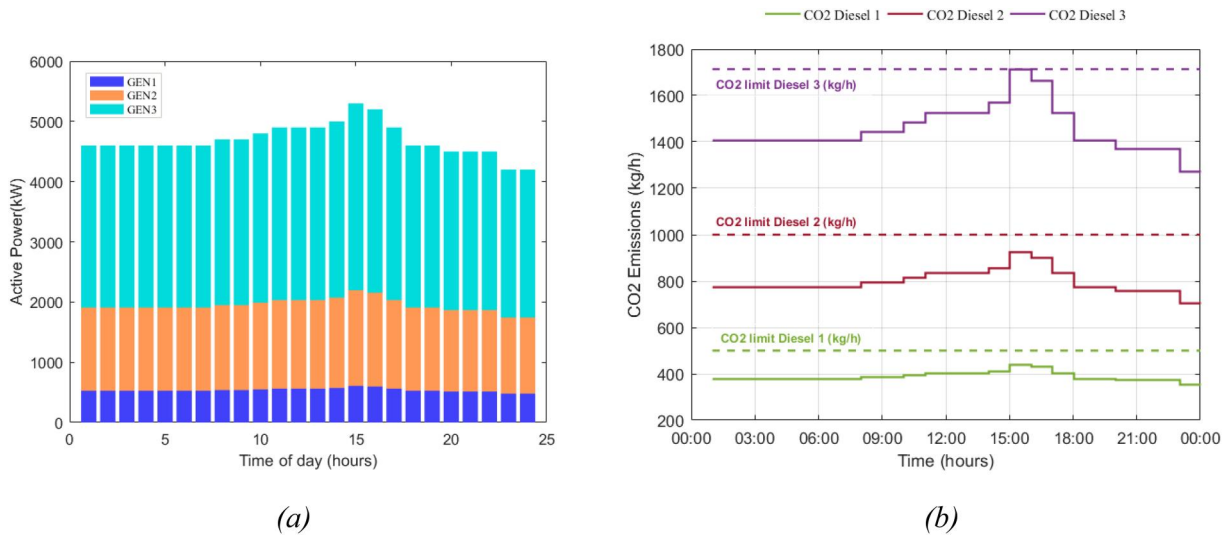

FIGURE 13 Auxiliary diesel generators (a) power produced and (b) CO_2 emissions with their upper limits (OSC II).

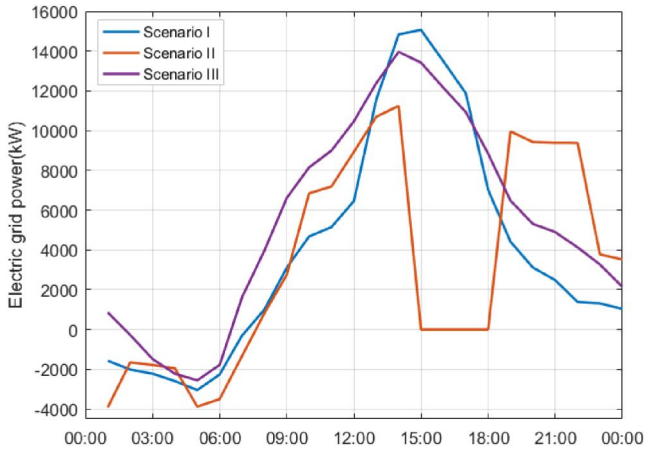

FIGURE 14 Active power exchanged by the electric grid and the microgrid (OSC I, II and III).

In OSC I, the PEVs consume a lot of energy from the main network during the same time period, while in OSC II, they inject power to the microgrid in order to supply microgrid loads. If microgrid's autonomous operation time period was different and coincided with a high electricity price period, the microgrid's daily operation cost would rise slightly. Finally, it is noted that the average time for the execution (load agents modelling, energy management level) of the proposed method was 3.5 min. This is a particularly low computation time since the method is applied to a highly complex optimisation problem with hundreds of thousands of decision variables and constraints while it allows its online application as it addresses a power and energy management problem. It should also be considered that the proposed method deals with a day-ahead operation scheduling and power management problem; hence, the required computation time is absolutely satisfactory. The average time for the execution of a traditional method (following the steepest gradient descent approach) was 1.2 min. However, the classical optimisation technique does not ensure convergence to a global optimum, as it depends highly on the selected initial point. Moreover, it was shown that our method managed to reduce the operation by 12.7% more than the classical method, on average.

The obtained results confirm that the efficient operation of a very complex microgrid comprising large-scale buildings, large number of hosted PEVs and RES with very small computation requirements is ensured by proposed method.

6 | CONCLUSION

An optimal operation scheduling method for complex microgrids comprising large-scale buildings, large number of PEVs and RES is proposed in this paper. Despite the complexity and the large size of the building prosumers the proposed method can exploit detailed integrated models of their thermal-electrical power systems. Moreover, an aggregation technique is applied to the hosted PEVs without compromising the accuracy of the results while ensuring large reduction of the required computation time. The proposed method can be applied to extremely complex building prosumers without the expected increase in the required computation time. The average time for the execution of the proposed method was 3.5 min. This is a particularly low computation time since the method is applied to a highly complex optimisation problem with hundreds of thousands of decision variables and constraints while it allows its online application as it addresses a power and energy management problem. This is achieved as an innovative method for the dispatch of total building thermal needs to the respective building thermal zones and is exploited in this work. Moreover, the proposed method can be applied to grid connected or islanded operation of the microgrid of building prosumers ensuring operation cost minimisation in both cases while PEVs are exploited as small power generation units during island operation. It is noted that the method is designed in a way that allows microgrid operation cost

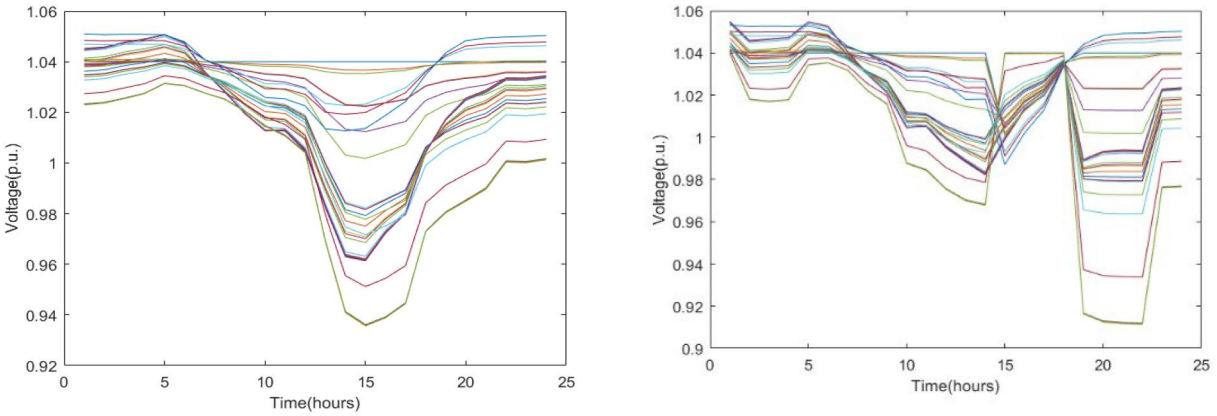

FIGURE 15 Node voltages (a) OSC I (b) OSC II.

minimisation together with the satisfaction of a huge number of microgrid components' constraints. The implementation of the method was based on the exploitation of a two-level hierarchical MAS.

A highly complex microgrid of large building prosumers, PEVs and RES was used to test the proposed method for different operation scenarios. In our case study, theoretically the decision variables amount up to 57,220. Detailed simulation results showed that operation cost savings, in the range of 27%, with regard to business-as-usual operation can be achieved. A cost increase of 6.32% between OSC I and II is obtained due to the fact that the microgrid is forced to operate autonomously in OSC II during 15:00–18:00 hrs, while the cost of electricity is at its lowest levels at this time. In OSC I, the PEVs absorb a large amount of energy power from the main grid during the same time period, whereas in OSC II, they inject power to the microgrid in order to supply microgrid loads. The cost of the microgrid's daily operation would increase slightly, in case the microgrid's autonomous operation period was shifted in time with a high electricity price period.

NOMENCLATURE

ABBREVIATIONS

EC	electric chiller
HVAC	heating, ventilation and air conditioning
MAS	multi-agent system
m.u.	monetary unit
PB	parking equivalent battery
PEV	plug-in electric vehicle
RES	renewable energy sources
SoC	state of charge
V2G	vehicle to grid

SETS AND INDICESS

$\mathcal{B}$, b	set of the buildings of the microgrid, index indicating the number of the building
$\mathcal{E}$	set of the external walls of each thermal zone
$\mathcal{G}$, g	set of the generators of the microgrid, index indicating the number of the diesel generator
$\mathcal{J}$	set of the internal walls of each thermal zone
$\mathcal{N}$	set of the neighboring thermal zones
x	index indicating the xth internal wall orientation
y	index indicating the yth external wall/window orientation
z	denotes the zth thermal zone of the building

PARAMETERS, CONSTANTS AND VARIABLES

β_z	surface slop
θ, θ_z	incidence, zenith angle, respectively
τ_{win}	the glass transmission coefficient of the windows
a_{0g}, a_{1g}, a_{2g}	coefficients of the gth generator fuel cost function
a_w	absorbance coefficient of the external surface of the wall
C_z	the specific heat capacity of the zth thermal zone
COP	HVAC performance coefficient
EP	the forecasted electricity price (m.u./kWh)
F_{wall}, F_{win}	the area of the total wall/window surface
FC	fuel cost function
I_b, I_d, I	beam, diffuse and total radiation on horizontal surface, respectively
$I_{T,z}$	the total solar radiation of the zth thermal zone
n_{ch}, n_{disch}	charging (discharging) efficiency coefficients of the PEV battery
n_{shift}	coefficient estimated by the optimal load shifting algorithm
N_g	number of the diesel generators of the microgrid

N_z	total number of the thermal zones of a building
p_g	ground reflectance
p	air density
P_{DNload}	distribution network load (kW)
$P_{EC,total,b}$	electric power consumed by the EC (kW)
$P_{EC,total,min}, P_{EC,total,max}$	lower and upper limits of the electric power consumed by the EC (kW)
P_g	power produced by the gth generator
$P_{g,min}, P_{g,max}$	minimum and maximum loading constraints of the gth diesel generator, respectively
$P^*_{non\_cr}$	the optimal electric power consumed by the non-critical loads of all buildings
$P_{PB,max}, P_{PB,min}$	maximum/minimum power transfer rate of the equivalent battery of the EV parking lot
P_{PV}	Forecasted power generation of the PV (kW)
P_{WT}	forecasted power generation of the WT (kW)
P_{grid}	power of the main electric grid (kW)
$Q_{EC,total}$	total cooling power of the building (kW)
$Q_{EC,z}$	cooling power generated by the EC of the zth thermal zone (kW)
$\dot{Q}_{ex,wall,z}$	heat transfer through the external walls of the zth thermal zone (kW)
$Q_{g,max}, Q_{g,min}$	upper and lower limits of the reactive power of the gth generator
$\dot{Q}_{in,wall,z}$	heat transfer through the internal walls of the zth thermal zone (kW)
$Q_{in,z}$	internal heat gains from people, appliances and lighting of the zth thermal zone (kW)
$Q_{PEV,max}, Q_{PEV,min}$	upper and lower limits of the reactive power of the PEVs' parking lot
$\dot{Q}_{sg,z}$	the whole solar radiation transmitted across the windows of the zth thermal zone (kW)
$\dot{Q}_{sw,z}$	heat contribution due to the solar radiation on the surface of the external walls of the zth thermal zone (kW)
$\dot{Q}_{win,z}$	heat transfer across the windows of the zth thermal zone (kW)
R_{se}	the external surface heat resistance for convection and radiation of the external wall
$T_{auto,0}, T_{auto,f}$	the beginning and the end of the time period where the microgrid operates autonomously
$T_{in,nz}$	indoor temperature of the neighbour thermal zone
$T_{in,z}$	indoor temperature (°C) of the zth thermal zone
$T_{max,z}, T_{min,z}$	the maximum and minimum values of the indoor temperature of the zth thermal zone (°C)
$t_{ON,g}, t_{OFF,g}$	time points that gth diesel generator starts, stops operating, respectively
$T_{ON\_min,g}, T_{OFF\_min,g}$	minimum allowable operation/non-operation time of the gth diesel generator
T_{out}	outdoor temperature (°C)
$T_{shift,0}, T_{shift,f}$	the beginning and the end of the time period where the non-critical loads can be shifted in time
SC	the shading coefficient of the windows
SoC_{PB}	SoC of the equivalent battery (kWh) of the EV parking lot
$SoC_{PB,max}, SoC_{PB,min}$	max/min stored energy (kWh) of the equivalent battery of the EV parking lot
$SoC_{0,PB}$	initial SoC (kWh) of the equivalent battery of the EV parking lot
$SoC_{t,PB}$	target energy (kWh) of the equivalent battery of the EV parking lot
U_{wall}, U_{win}	heat transfer coefficient of the external wall/window of the thermal zone
V_z	volume of the air of the zth thermal zone

CONFLICT OF INTEREST STATEMENT

The authors declare no conflicts of interest.

DATA AVAILABILITY STATEMENT

Research data are not shared.

ORCID

Fotios D. Kanellos https://orcid.org/0000-0003-0433-1395

REFERENCES

1. Thomas, D., Deblecker, O., Ioakimidis, C.S.: Optimal operation of an energy management system for a grid-connected smart building considering photovoltaics' uncertainty and stochastic electric vehicles' driving schedule. Appl. Energy 210, 1188–1206 (2018). https://doi.org/10.1016/j.apenergy.2017.07.035
2. Ma, Y., Matusko, J., Borrelli, F.: Stochastic model predictive control for building HVAC systems: complexity and conservatism. IEEE Trans. Control Syst. Technol. 23(1), 101–116 (2015). https://doi.org/10.1109/tcst.2014.2313736
3. Sturzenegger, D., et al.: Model predictive climate control of a Swiss office building: implementation, results, and cost-benefit analysis. IEEE Trans. Control Syst. Technol. 24(1), 1–12 (2016). https://doi.org/10.1109/tcst.2015.2415411

4. Carli, R., Dotoli, M.: Decentralized control for residential energy management of a smart users' microgrid with renewable energy exchange. IEEE/CAA J. Automatica. Sinica. 6(3), 641–656 (2019). https://doi.org/10.1109/jas.2019.1911462
5. Alibabaei, N., et al.: Effects of intelligent strategy planning models on residential HVAC system energy demand and cost during the heating and cooling seasons. Appl. Energy 185, 29–43 (2017). https://doi.org/10.1016/j.apenergy.2016.10.062
6. Arcos-Aviles, D., et al.: Fuzzy logic-based energy management system design for residential grid-connected microgrids. IEEE Trans. Smart Grid 9(2), 530–543 (2018). https://doi.org/10.1109/tsg.2016.2555245
7. Zhang, C., et al.: Robust operation of microgrids via two-stage coordinated energy storage and direct load control. IEEE Trans. Power Syst. 32(4), 2858–2868 (2017). https://doi.org/10.1109/tpwrs.2016.2627583
8. Sehar, F., Pipattanasomporn, M., Rahman, S.: Coordinated control of building loads, PVs and ice storage to absorb PEV penetrations. Int. J. Electr. Power Energy Syst. 95, 394–404 (2018). https://doi.org/10.1016/j.ijepes.2017.09.009
9. Liang, Z., et al.: Optimal energy management for commercial buildings considering comprehensive comfort levels in a retail electricity market. Appl. Energy 236, 916–926 (2019). https://doi.org/10.1016/j.apenergy.2018.12.048
10. Liu, N., et al.: Multiparty energy management for grid-connected microgrids with heat- and electricity-coupled demand response. IEEE Trans. Ind. Inf. 14(5), 1887–1897 (2018). https://doi.org/10.1109/tii.2017.2757443
11. Abou Houran, M., et al.: Economic dispatch of grid-connected microgrid for smart building considering the impact of air temperature. IEEE Access 7, 70332–70342 (2019). https://doi.org/10.1109/access.2019.2915528
12. Zhang, Y., Gatsis, N., Giannakis, G.B.: Robust energy management for microgrids with high-penetration renewables. IEEE Trans. Sustain. Energy 4(4), 944–953 (2013). https://doi.org/10.1109/tste.2013.2255135
13. Zheng, Y., Li, S., Tan, R.: Distributed model predictive control for on-connected microgrid power management. IEEE Trans. Control Syst. Technol. 26(3), 1028–1039 (2018). https://doi.org/10.1109/tcst.2017.2692739
14. Jiang, Q., Xue, M., Geng, G.: Energy management of microgrid in grid-connected and stand-alone modes. IEEE Trans. Power Syst. 28(3), 3380–3389 (2013). https://doi.org/10.1109/tpwrs.2013.2244104
15. Li, Z., Xu, Y.: Optimal coordinated energy dispatch of a multi-energy microgrid in grid-connected and islanded modes. Appl. Energy 210, 974–986 (2018). https://doi.org/10.1016/j.apenergy.2017.08.197
16. Guo, Y., Zhao, C.: Islanding-aware robust energy management for microgrids. IEEE Trans. Smart Grid 9(2), 1301–1309 (2018). https://doi.org/10.1109/tsg.2016.2585092
17. Pinzon, J.A., et al.: Optimal management of energy consumption and comfort for smart buildings operating in a microgrid. IEEE Trans. Smart Grid 10(3), 3236–3247 (2019). https://doi.org/10.1109/tsg.2018.2822276
18. Pinzon, J.A., et al.: A MILP model for optimal management of energy consumption and comfort in smart buildings. In: 2017 IEEE Power and Energy Society Innovative Smart Grid Technologies Conference, ISGT (2017)
19. Hao, H., et al.: Transactive control of commercial buildings for demand response. IEEE Trans. Power Syst. 32(1), 774–783 (2017). https://doi.org/10.1109/tpwrs.2016.2559485
20. Cui, Q., et al.: Effect of device models on the multiobjective optimal operation of CCHP microgrids considering shiftable loads. Appl. Energy 275, 115369 (2020). https://doi.org/10.1016/j.apenergy.2020.115369
21. Bharati, G.R., et al.: Hierarchical optimization framework for demand dispatch in building-grid systems. In: IEEE Power and Energy Society General Meeting (2016)
22. Anvari-Moghaddam, A., et al.: A multi-agent based energy management solution for integrated buildings and microgrid system. Appl. Energy 203, 41–56 (2017). https://doi.org/10.1016/j.apenergy.2017.06.007
23. Liu, Z., et al.: Energy storage capacity optimization for autonomy microgrid considering CHP and EV scheduling. Appl. Energy 210, 1113–1125 (2018). https://doi.org/10.1016/j.apenergy.2017.07.002
24. Tavakoli, M., et al.: A two stage hierarchical control approach for the optimal energy management in commercial building microgrids based on local wind power and PEVs. Sustain. Cities Soc. 41, 332–340 (2018). https://doi.org/10.1016/j.scs.2018.05.035
25. Eseye, A.T., et al.: Optimal energy trading for renewable energy integrated building microgrids containing electric vehicles and energy storage batteries. IEEE Access 7, 106092–106101 (2019). https://doi.org/10.1109/access.2019.2932461
26. Santos, A., et al.: Summary of Travel Trends: 2009 National Household Travel Survey. U.S. Dept. Transp., Federal Highway Admin (2011). Tech. Rep http://nhts.ornl.gov/2009/pub/stt.pdf
27. Jin, X., et al.: Hierarchical microgrid energy management in an office building. Appl. Energy 208, 480–494 (2017). https://doi.org/10.1016/j.apenergy.2017.10.002
28. Kyriakou, D.G., Kanellos, F.D.: Optimal operation of microgrids comprising large building prosumers and plug-in electric vehicles integrated into active distribution networks. Energies 15(17), 6182 (2022). https://doi.org/10.3390/en15176182
29. Farinis, G.K., Kanellos, F.D.: Integrated energy management system for Microgrids of building prosumers. Elec. Power Syst. Res. 198, 107357 (2021). https://doi.org/10.1016/j.epsr.2021.107357
30. Kanellos, F.D., et al.: Efficient and robust power and energy management for large clusters of plug-in electric vehicles and distribution networks. IET Energy Syst. Int. 4(3), 393–408 (2022). https://doi.org/10.1049/esi2.12070
31. Kanellos, F.D.: Optimal power management with GHG emissions limitation in all-electric ship power systems comprising energy storage systems. IEEE Trans. Power Syst. 29(1), 330–339 (2014). https://doi.org/10.1109/tpwrs.2013.2280064
32. Kanellos, F.D.: Optimal scheduling and real-time operation of distribution networks with high penetration of plug-in electric vehicles. IEEE Syst. J. 15(3), 3938–3947 (2021). https://doi.org/10.1109/jsyst.2020.3006002

How to cite this article: Kyriakou, D.G., Kanellos, F. D.: Energy and power management system for microgrids of large-scale building prosumers. IET Energy Syst. Integr. 5(2), 228–244 (2023). https://doi.org/10.1049/esi2.12095